

Modelling and control of electric vehicle power train

Souhir Tounsi

National School of Electronics and Telecommunications of Sfax-(SETIT): Research Unit, Sfax University, Sfax, Tunisia

Email address:

souhir.tounsi@isecs.rnu.tn

To cite this article:

Souhir Tounsi. Modelling and Control of Electric Vehicle Power Train. *American Journal of Electrical Power and Energy Systems*. Special Issue: Design, Optimization and Control of Electric Vehicles: (DOCEV). Vol. 4, No. 2-1, 2015, pp. 33-41.

doi: 10.11648/j.epes.s.2015040201.15

Abstract: This paper describes the choice and the design of electric vehicles power train structure reducing considerably the energy consumption. Indeed The converter feeding the motor is naturally with IGBTs leading on the one hand to important losses and on the other hand to many control problems. This structure is replaced by another with electromagnetic switch leading to a strong reduction of the losses and to an increase of the electric motor control reliability. The power train contains an energy recuperation system during the deceleration phases, where the motor functions in generator. The motor is controlled by vector control method maintaining the current I_d equal to zero, leading to the maintain of the current in phase with electromotive force, what also leads to the reduction of the energy consumption. A super-capacity is added in parallel with the energy accumulator leads to an increase of the storage energy capacity. All these factors lead to the increase of the autonomy for a known stocked energy.

Keywords: Power Chain, Design, Battery, Converter, Thermal Model, Simulation

1. Introduction

Currently and in look of the strong petroleum crises, during these last decades and the problems of atmospheric pollution, the electrification of the vehicles project became a project of actuality. In this context, several works of research are thrown on this thematic [1], [2], [3], [4] and [5].

Following several works of research a single motor configuration provided with a differential is kept. The motor is with permanent magnet and sinusoidal wave-form, having an axial structure. Naturally the power converter is with IGBTs, leading to an important energy losses [6], and to many control problems: such as the floating voltage and the tail current at the commutation time and the problems of the static and dynamic latch-up requiring a complicating control system. In our case, we choices a static converter structure with electromagnetic switch leading practically to the annulment of losses and to the increase of the reliability of the control.

The power train includes an energy recuperation system during decelerations phases leading to the reduction of the energy consumption and thereafter to the increase of the autonomy.

We choices a vector control strategy fixing the electromotive force in phase with the current (Strategy $I_d = 0$) also leading to the economy of energy and thereafter the

increase of the autonomy. The design of this power train takes in account of most technological constraints and others attached to reliability [6].

This paper describes the choice, the design methodology and the control strategy of this power train.

2. Electric Vehicle Power Train Structure

The synoptical schema of the electric vehicle power train is illustrated by figure1:

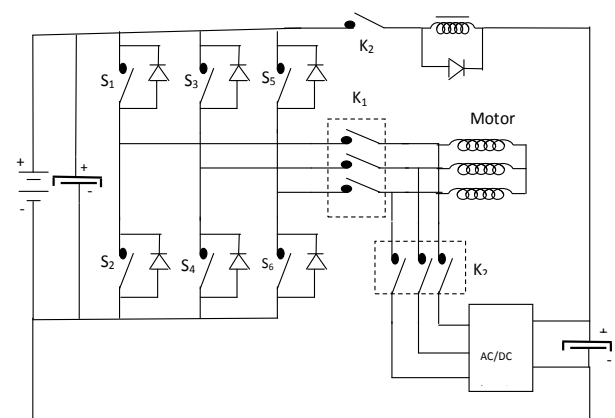


Figure 1. Electric vehicle power train structure.

Naturally, DC/AC converter powering the motor is with IGBTs. In our case, we have chosen a structure with electromagnetic switches leading to a reduction of the energy losses. The control of these switches is assured by six generating windings. Being powered by a sufficient current, these windings attract their ferro-magnetic cores, leading to the closings of these switches according to the vector control strategy fixing the current in phase with the electromotive force ($I_d = 0$). At the time of their dice-power these windings free the energy stocked through a free wheel diode. Two working phases are possible:

- Working in motor phase: in this phase the K1 switches are closed and generating windings assures the opening and the closing of the converter's switches according to a vector control strategy reducing the energy consumption. This phase is possible for working either in accelerated phase or in constant speed. During this phase the K2 switches are open.

- Working in generating phase: this phase is possible for a working in decelerated phase. In this phase, the motor function in generator. The control system opens the switches of the static converter and the K1 switches. At this moment the energy recuperation system functions. In this phase, the K2 switches close itself to convert the three electromotive forces of the motor that absorbed himself according to the speed decreasing during the time on DC voltage. The recovered DC voltage is filtered by a capacitor. This voltage source is converted in a current source permitting the injection of electrons in the battery. This last is in charge thereafter. This phase is named energy recuperation phase. The duration of this phase is until the stability of the speed or the acceleration of the vehicle.

3. Dimensioning Torque Energy Accumulator

The energy accumulator is a coupling of several elementary batteries, whose structure is given by the figure 2:

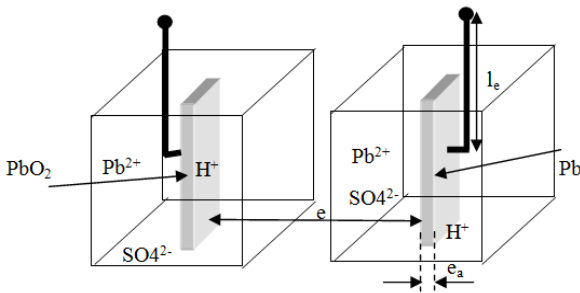


Figure 2. Elementary structure of battery.

Every element is composed of reservoirs with different electric polarity, in contact with two armatures. This structure is equivalent to a capacity temporarily charged by the quantity of charge recovered by the armature. Two electrodes permit the recuperation of the voltage generated by the battery. The whole armature more electrodes present a resistance in series with the capacity. A capacity in parallel with this resistance

exists. The existence of this capacity can be explained by the polarity difference between electrode-armature and electrode output voltage contacts, what leads to the equivalent diagram of a battery element (figure3):

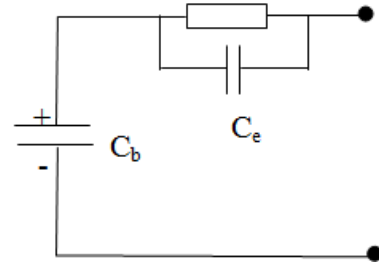


Figure 3. Model of the battery elementary structure

$$C_b = \frac{\epsilon e}{S_a} \quad (1)$$

Where ϵ and e are respectively the permittivity and the distance of the place separating the armatures and S_a is the surface of the armature.

$$C_e = \frac{\epsilon l_e}{S_e} \quad (2)$$

l_e and S_e are respectively the length and the section of one electrode.

$$R_b = 2 \frac{\rho_a(t) e_a}{S} + 2 \frac{\rho_e(t) l_e}{S_e} \quad (3)$$

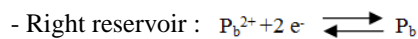
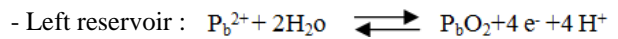
Where ρ_a and ρ_e are respectively the materials resistivity of the armature and the electrode, S is the section of armature and e_a is the armature thickness.

The number of elements in series and in parallel depends on the stocked energy and on the battery delivered voltage. We expect the coupling of a super-capacitor in parallel with the battery to increase the storage capacity of the accumulator of energy. If we disregard R_b and C_e , the energy stocked in the accumulator is deduced by the following formula:

$$W_b = \frac{1}{2} (C_{bt} + C_s) U_b^2 \quad (4)$$

Where C_{bt} and C_s are respectively the equivalent capacities of the battery and the super-capacity and U_b is the battery voltage.

The equation of oxydo-reduction is as follow:



$[H^+]$ and $[Pb^{2+}]$ are the molar concentrations of hydrogen and lead.

The voltage to the level of the two electrodes left and right are given by the following NRENST formula:

$$E_G = E_G^0 + \frac{R \times T}{2 \times A} \times \ln([Pb^{2+}]) \quad (5)$$

$$E_D = E_D^0 + \frac{R \times T}{2 \times A} \times \ln \left(\frac{[H^+]^4}{[P_b^{2+}]^2} \right) \quad (6)$$

Where E_G^0 and E_D^0 are the standard voltages of the two red-ox couples, T is the temperature and R , A are constants.

From where the difference of the two electrodes voltages is expressed by the following formula:

$$U_e = E_D^0 - E_G^0 + \frac{R \times T}{2 \times A} \times \ln \left(\frac{[H^+]^4}{[P_b^{2+}]^2} \right) - \frac{R \times T}{2 \times A} \times \ln ([P_b^{2+}]) \quad (7)$$

At 25°C the voltage of one element of battery is expressed as follow:

$$U_e = E_D^0 - E_G^0 + \frac{0.06}{2} \times \ln \left(\frac{[H^+]^4}{[P_b^{2+}]^2} \right) \quad (8)$$

The number of elements to couple in series to get the wished battery voltage is deducted therefore from the following formula:

$$n_{es} = \frac{U_b}{E_D^0 - E_G^0 + \frac{0.06}{2} \times \ln \left(\frac{[H^+]^4}{[P_b^{2+}]^2} \right)} \quad (9)$$

The number of elements to couple in parallel to complete the stocked energy reserves is expressed as follow:

$$n_{ep} = \frac{W_b - \left(\frac{1}{2} \times n_{es} \times C_e \times U_e^2 + \frac{1}{2} \times C_s \times U_b^2 \right)}{\frac{1}{2} \times C_e \times U_e^2} \quad (10)$$

4. Design Methodology of Electric Motor

The chosen of electric motor structures is oriented to permanent magnets, axial flux and modular structure with more combination and its radial flux equivalent motor [7].

Figure 4 illustrates one configuration with axial flux and its radial flux equivalent structure:

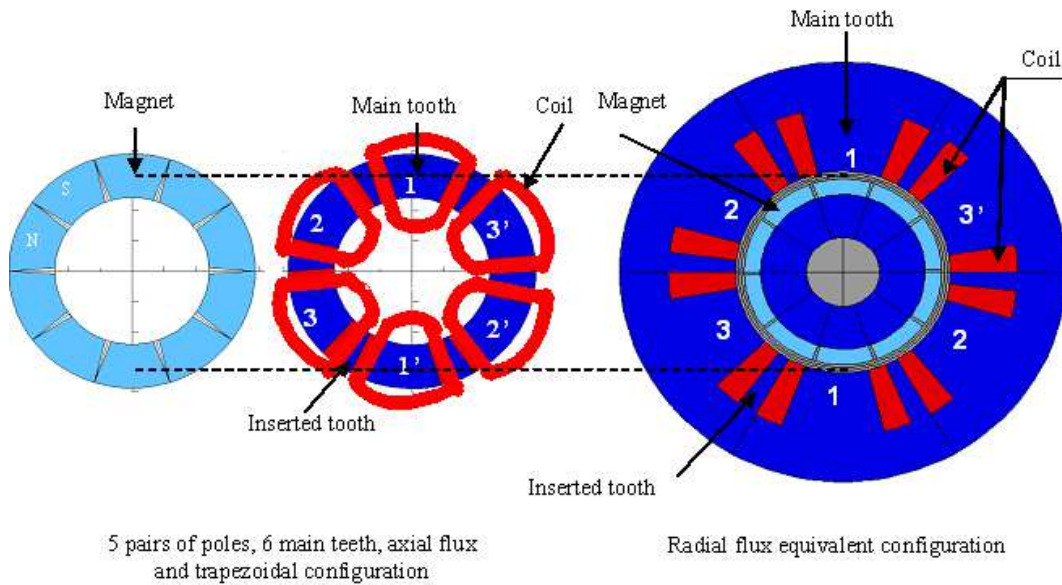


Figure 4. Example of motor configuration.

The design methodology consists of the determination of geometrical and control parameters of the motor-converter improving Autonomy. The motor must function on a broad beach of speed and without demagnetization. This methodology requires the development of an analytical and parameterized model of the all motor-converter. This latter last makes it possible to establish the relation between data, such as: the data of schedule conditions, the constant characterizing materials, the expert data, the motor configuration and the outputs such as: geometrical and electromagnetic motor magnitudes [8].

This model is validated by finite elements method [8].

Indeed, the motor is drawn according to its geometrical magnitudes extracted from analytical model with the software Maxwell-2d, and is simulated in dynamic and static in order to compare the results obtained with those found by the analytical method.

The coupling of this model to a model evaluating the autonomy poses an optimization problem with several variables and constraints. This latter is solved by the genetic algorithms (GAs) method [9].

The global architecture of the design methodology is illustrated in figure 5.

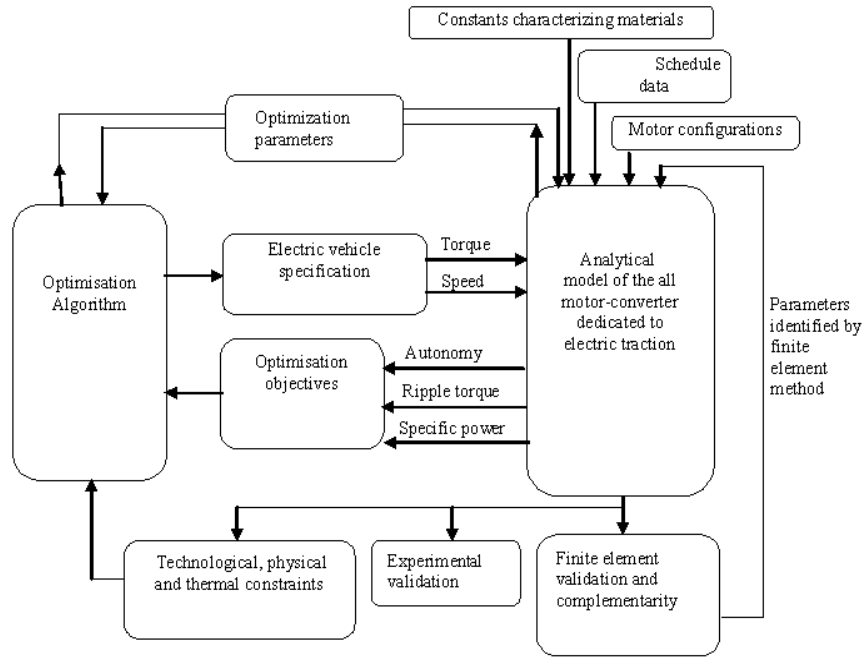


Figure 5. Design methodology of traction motor.

The structure of the motor is modular that is to say multi-stages. The design analytic model of the motor is found on [7].

A thermal nodal model of the electric motor is developed to respect thermals constraints [8]. This thermal model of the

motor modular structure is developed while considering that the flux of heat propagates itself axially. The figure 6 illustrates this property:

The nodal model of the motor structure is illustrated by the figure 7:

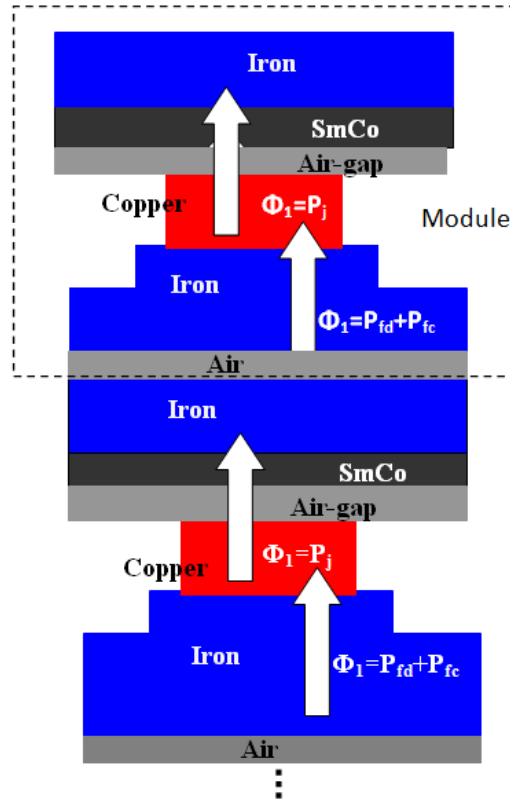


Figure 6. Thermal flux propagation.

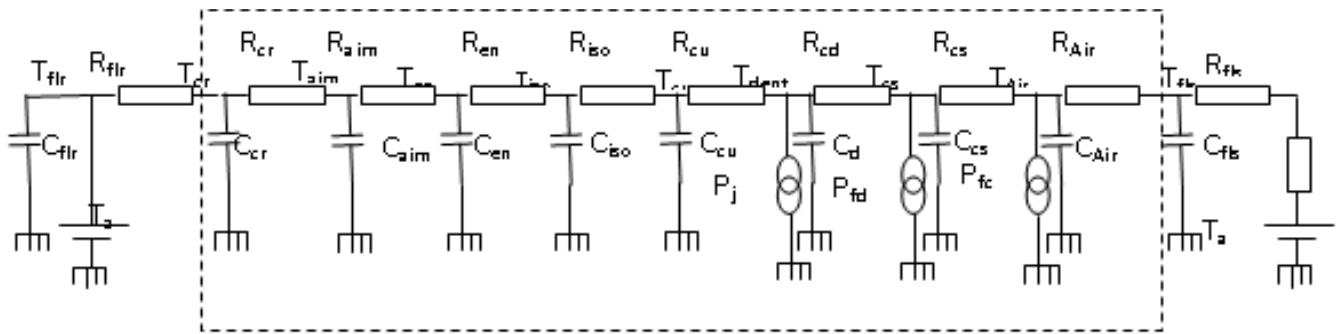


Figure 7. Thermal model of the motor structure.

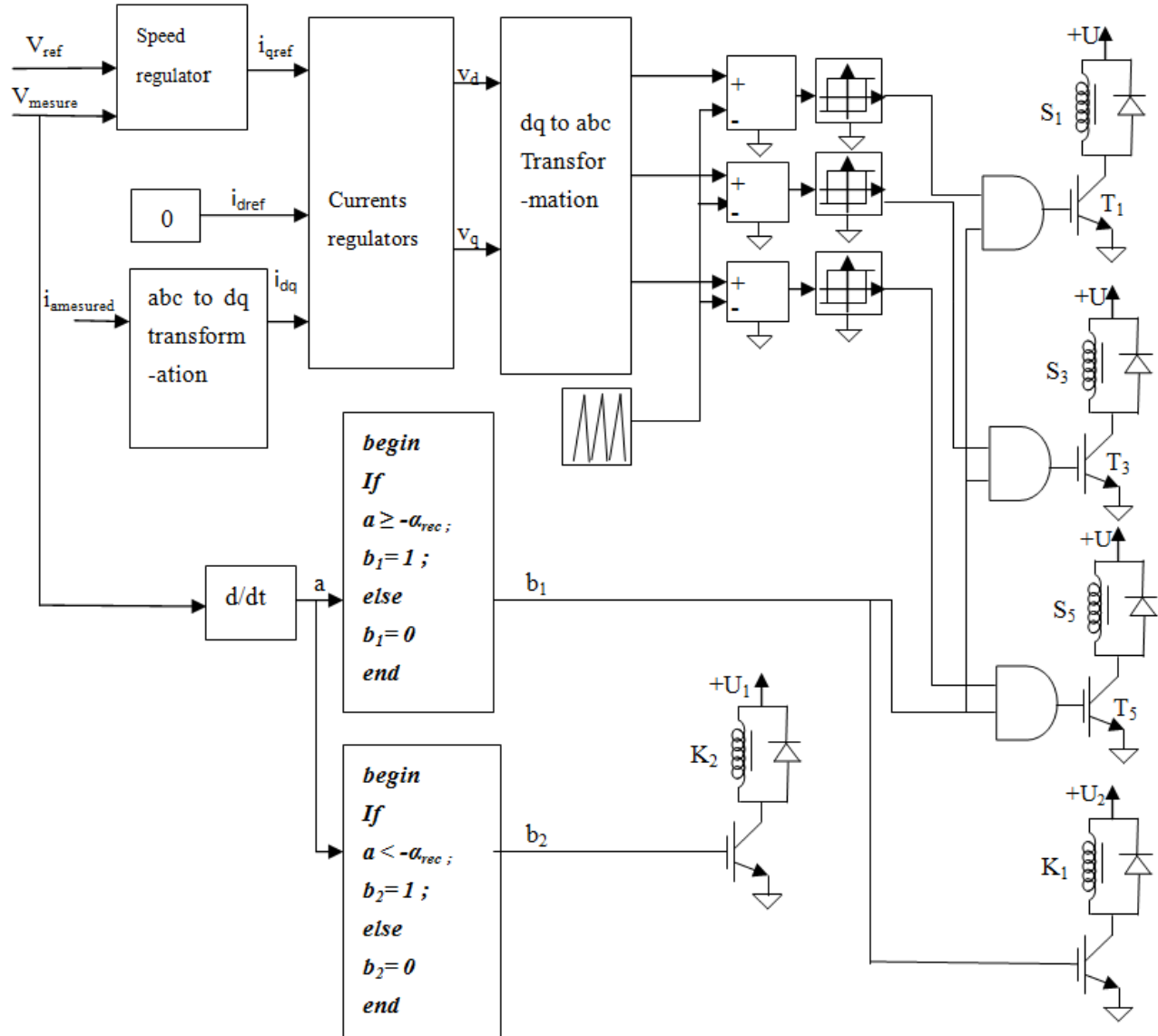


Figure 8. Control generator structure.

Table 1. illustrates the nomenclature of the nodal model diagram

h_l	Free convection coefficient
S_r	Active section of the rotor
h_f	Forced convection coefficient
S_s	Active section of the stator
R_{cr}	Rotor yoke conduction resistance
R_c	Magnets conduction resistance
R_{ce}	Air-gap conduction resistance
R_{cu}	Copper conduction resistance
R_{cd}	Teeth conduction resistance
R_{cs}	Stator yoke conduction resistance
R_{Air}	Air conduction resistance
P_j	Copper losses
P_{fd}	Teeth iron losses
P_{fc}	Stator yoke iron losses
T_a	Ambient temperature
T_{cr}	Rotor yoke temperature
T_{ai}	Magnets temperature
T_{en}	Air-gap temperature
T_{cu}	Copper temperature
T_d	Teeth temperature
T_{cs}	Stator yoke temperature
C_{cr}	Thermal capacity of the rotor yoke
C_{aim}	Thermal capacity of magnets
C_{en}	Thermal capacity of the air-gap
C_{cu}	Thermal capacity of the copper
C_d	Thermal capacity of the teeth
C_{cs}	Thermal capacity of the stator yoke
C_{Air}	Thermal capacity of the air
C_{iso}	Thermal capacity of insulation

5. Control Generator Structure

The control generator structure is illustrated by figure 8.

The control generator assures the transmission of the control signals to the T1 transistors, T3 and T5 dragging the excitation respectively of the three generating windings S1, S3 and S5 according to the vector control law ($I_d=0$ strategy) during the phases of working to constant speed or in accelerated phase. These three windings attract their cores according to the nature of control signals. Three other windings S2, S4 and S5, no schematized in the control circuit will be powered by signals complementary respectively to the control signals: S1, S3 and S5.

During the energy recuperation phase, b1 signals drags the opening of the DC/AC converter switches and the opening of the K1 switches. b2 signal drags the closing of the K2 switches following the excitation of the K2 winding. This phase is only possible for decelerations lower to a doorstep where the recuperation is not negligible.

The model of the control generator is implanted under Matlab/Simulink environment (figure 9).

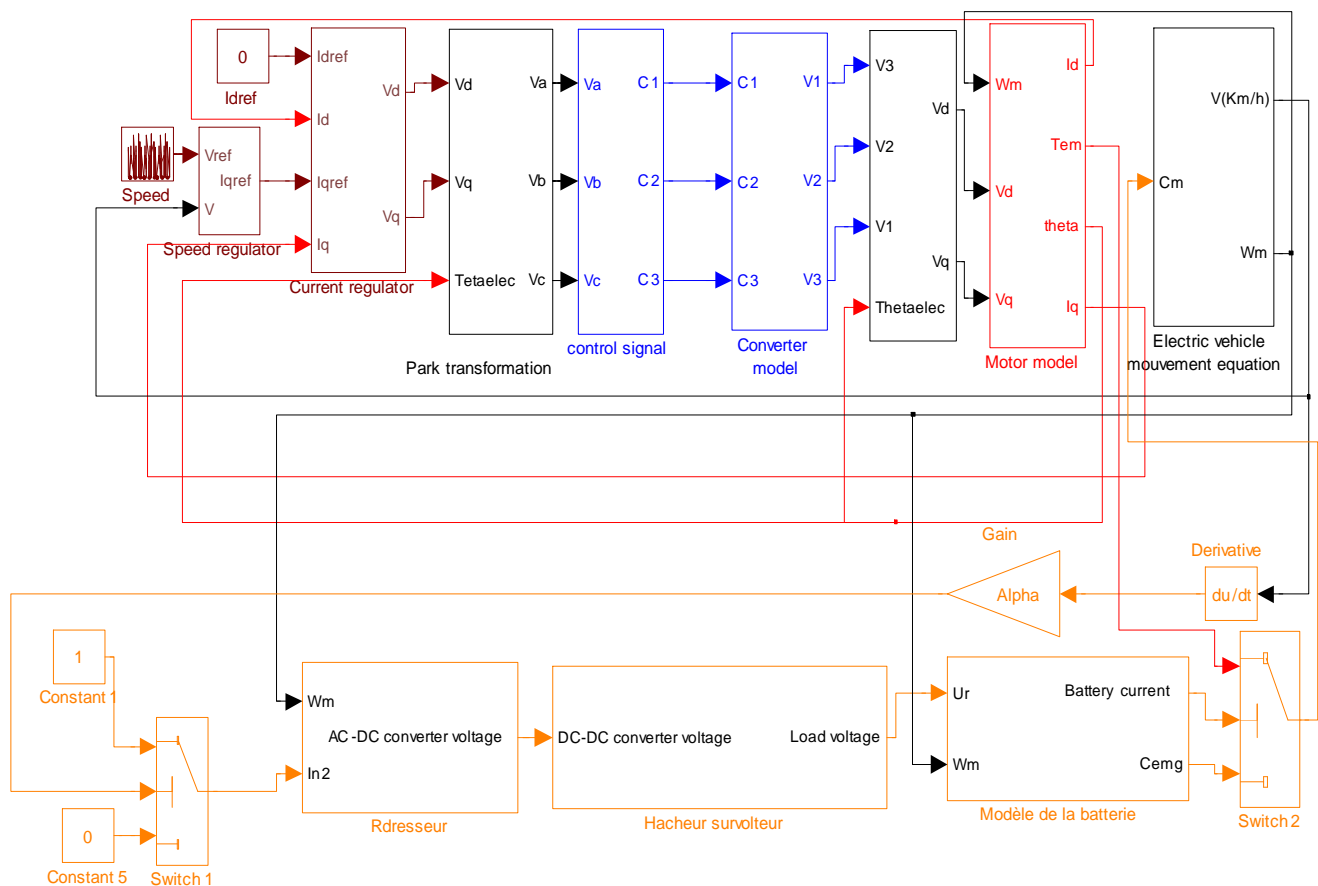


Figure 9. Simulink model of the control generator.

6. Generating Winding

The generating windings assure the closing and the opening of DC/AC converter electromagnetic switches, according to the chosen of control law. When a winding is powered by a sufficient current, it attracts its core and drags the closing of one or switches attached to its Ferro-magnetic core thereafter. The current powering this windings, must be sufficient to defeat the opposite strength generated by the recall spring.

The structure of the generating winding is illustrated by the figure 10:

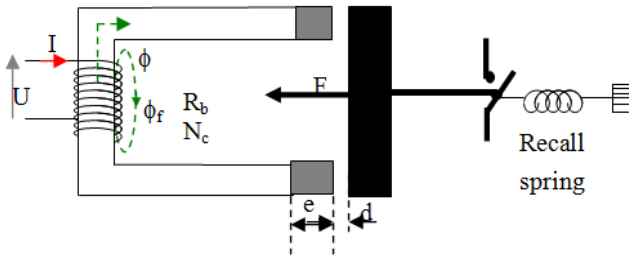


Figure 10. Generating winding.

The generating winding inductance depends on the displacement of the mobile iron core:

$$L_b = \frac{N_c^2}{\mathfrak{R}_t} = \frac{N_c^2}{\frac{2 \times e}{\mu_0 \times S} + \frac{2 \times (d-x)}{\mu_0 \times S}} = \frac{\mu_0 \times S \times N_c^2}{2 \times (e+d-x)} \quad (11)$$

Where N_c is the spires number of winding, μ_0 is the air permeability, S is the section of the iron core, x is the displacement of the iron core.

The energy stocked in the winding is given by the following equation:

$$W = \frac{1}{2} \times L_b \times I^2 \quad (12)$$

The power drifting of this energy is given by the following equation:

$$P = \frac{dW}{dt} = \frac{I^2 \times \mu_0 \times S \times N_c^2}{4} \times \frac{d}{dt} \left(\frac{1}{e+d-x} \right) \quad (13)$$

This electric power turns into a mechanical power to the level of the mobile iron core:

$$P = F \times V \quad (14)$$

Where F and V are respectively the attraction strength and the speed of the mobile iron core.

We deduct from the two equations (13) and (14) the expression of the attraction strength depending on the displacement x :

$$F = \frac{\mu_0 \times U^2 \times S \times N_c^2}{R_b^2} \times \frac{d}{dx} \left(\frac{1}{e+d-x} \right) = \frac{\mu_0 \times U^2 \times S \times N_c^2}{R_b^2} \times \left(\frac{1}{(e+d-x)^2} \right) \quad (15)$$

The equation that describes the working of the mobile iron core and switch, drift of the dynamics fundamental relation:

$$M_n \times \frac{dV}{dt} = F - m \times K \times x \quad (16)$$

Where M_n is the mass of the mobile iron core, K is recall spring constant and m is the number of attracted switches.

While replacing F by its expression, (16) becomes:

$$M_n \times \frac{dV}{dt} = \frac{\mu_0 \times U^2 \times S \times N_c^2}{R_b^2} \times \left(\frac{1}{(e+d-x)^2} \right) - m \times K \times x \quad (17)$$

At the balance we have:

$V = 0$ and $d = x$, from where we deduct the expression of the powering voltage:

$$U = \sqrt{\frac{4 \times m \times K \times e^2 \times R_b^2}{\mu_0 \times S \times N_c^2}} \quad (18)$$

The active section of the copper depends on the admissible current density in the copper:

$$S_c = \frac{I}{\delta} = \frac{U}{R_b \times \delta} \quad (19)$$

From the equations (18) and (19) we deduct the expression of the active section of winding copper thread:

$$S_c = \sqrt{\frac{4 \times m \times K \times e^2}{\mu_0 \times \delta^2 \times S \times N_c^2}} \quad (20)$$

The generating winding resistance is given by the following equation:

$$R_b = \frac{\rho \times L_e}{S_c} \quad (21)$$

Where ρ is the copper resistivity and L_e is the winding length:

$$L_e = 2 \times N_{c/c} \sum_{n=1}^{N_{cc}} \left(a + b + 2 \times n \times \sqrt{\frac{S_c}{\pi}} \right) \quad (22)$$

Where N_c is the total number of winding spires, $N_{c/c}$ is the number of thread layer rolled up, a and b are respectively the iron core width and thickness.

$$N_{c/c} = \frac{E_B}{2 \times \sqrt{\frac{S_c}{\pi}}} \quad (23)$$

Where E_B is the thickness of the copper thread rolled up.

The number of thread by layer is given by the following equation:

$$N_{cc} = \frac{N_c}{N_{c/c}} \quad (24)$$

From where the winding resistance is deduced by the following equation:

$$R_b = \frac{\rho \times \left(2 \times N_{c/c} \sum_{n=1}^{N_{cc}} \left(a + b + 2 \times n \times \sqrt{\frac{4 \times m \times K \times e^2}{\mu_0 \times \delta^2 \times S \times N_c^2}} \right) \right)}{\sqrt{\frac{4 \times m \times K \times e^2}{\mu_0 \times \delta^2 \times S \times N_c^2}}} \quad (25)$$

7. Simulation Results

The model of the losses is implanted under the environment of Matlab/Simulink. The thermal fluxes are calculated while leaning on the inverse gait of modelling of the power chain.

The simulation of the thermal model with a natural ventilation (Coefficient of convection equal to 30 W/m²K) and for a working to speed consolidated equal to 80 km/h, give the evolution of the temperatures in the different active parts of the motor (figure11).

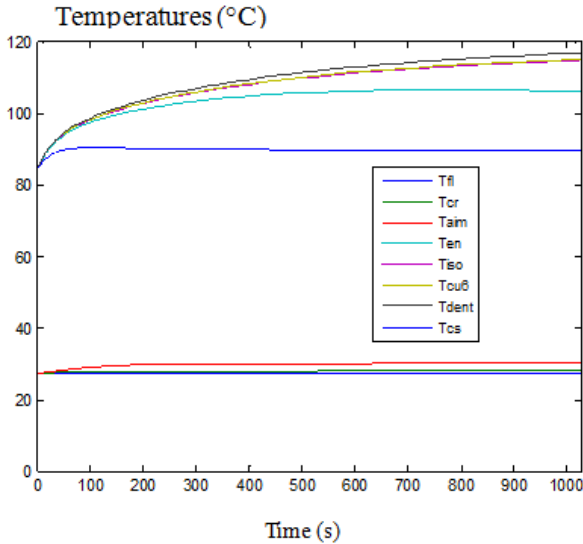


Figure 11. Evolution of the temperatures in the different active parts of the motor for a speed consolidated of 80 km/h ($h=30$ W/m²K).

Where T_{fl} is the average temperature of flabby, T_{cr} is the average temperature of the rotor yoke, T_{aim} is the average temperature of magnet, T_{en} is the average temperature of air-gap, T_{iso} is the average temperature of isolating, T_{cu} is the

average temperature of copper, T_{dent} the average temperature of stator teeth and T_{cs} the average temperature of the stator yoke.

This face shows that there is an overtaking of 47 °C for the copper and the resin, what proves the necessity of a cooling system. Several simulations are thrown for several values of forced convection coefficient to a system of cooling by forced ventilation, led to the fixing of this coefficient to 300 W/m²K.

The evolution of the temperatures in the different active parts of the motor for a working with a system of cooling to forced ventilation with a convection coefficient equal to 300 W/m²K is illustrated by the figure 12.

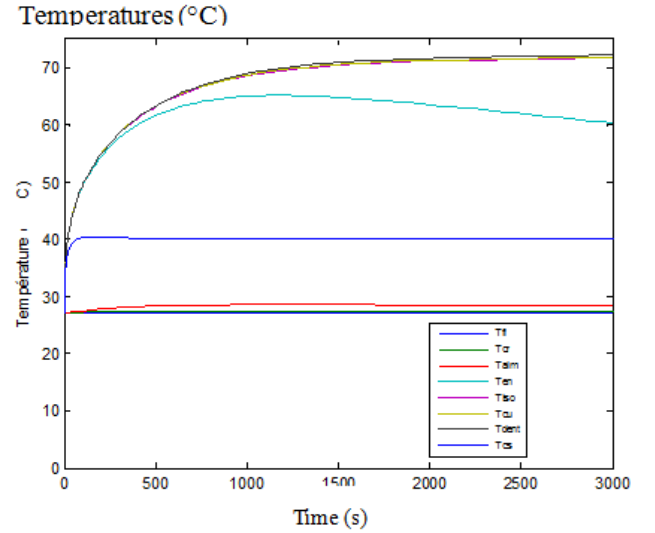


Figure 12. Evolution of the temperatures in the different active parts of the motor for a speed consolidated to 80 km/h ($h=300$ W/m²K).

The energy recovered (figure 13) believes at the time of the phases of strong decelerations and remain constant during the phases of working in motor.

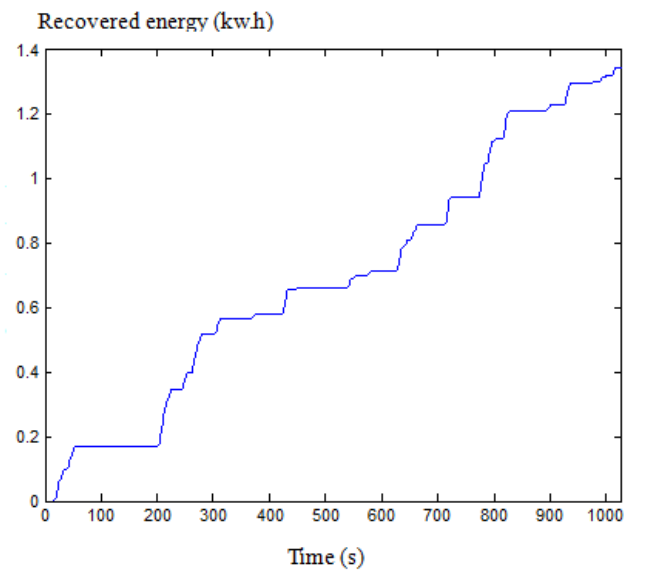


Figure 13. Recovered energy.

This energy is equal in middle value to 0.6942 kw.h on a

duration of 1027 s. This value is important, what shows the efficiency of the system of energy recuperation.

8. Conclusion

The choice done, the design methodology and control of this power train, increases the autonomy, reliability, considerably. This power train structure presents an attractive solution to solve the problem of the electric vehicles weak autonomies. It's interesting to study the problem of the excessive cost and the problem of battery load infrastructure in future.

List of Symbols

Cb	Elementary battery capacity
Ce	Electrode armature capacity
ε	Permittivity of the place separating the armatures
e	Length of the place separating armatures
le	Length of electrode
Sa	Armature section
Se	Electrode section
pa	Resistivity of the armature material
pe	Resistivity of the electrode material
Wb	Energy stocked in the accumulator
Rb	Armature-electrode resistance
Cbt	Equivalent capacity of the battery
Cs	Super-capacity
Ue	Voltage of elementary battery
nes	Number of elementary battery coupled in series
nep	Number of elementary battery coupled in parallel
Pj	Copper losses
Pfd	Iron losses in teeth
Pfc	Iron losses in stator yoke
Ta	Ambient temperature
Lb	Winding inductance
Nc	Spires number
μ_0	Air permeability
S	Section of iron core
x	Displacement of iron core
W	Energy stocked in winding
I	Current feeding the winding
P	Electric power of the winding
F	Attraction iron core strength
U	Voltage feeding the winding
Mn	Mass of the mobile iron core
K	Recall spring constant
V	Velocity of the mobile iron core
m	Number of attracted switches

Sc	Active section of the copper
δ	Current density
Nc	Number of winding spires
Nc/c	Number of thread layer rolled up
Ncc	Number of thread by layer
EB	Thickness of the copper thread rolled up

References

- [1] Naomitsu Urasaki, Tomonobu Senjyu and Katsumi Uezato: "A novel calculation method for iron loss resistance suitable in modelling permanent-magnet motors", IEEE TRANSACTION ON ENERGY CONVERSION, VOL. 18. NO 1, MARCH 2003.
- [2] B. Ben Salah, A. Moalla, S. Tounsi, R. Neji, F. Sellami: "Analytic design of Permanent Magnet Synchronous motor Dedicated to EV Traction with a Wide Range of Speed Operation", Internéational Review of Electrical Engineering (I.R.E.E), VOL 3, NO 1 January-February 2008"
- [3] Sid Ali. RANDI : Conception systématique de chaînes de traction synchrones pour véhicule électrique à large gamme de vitesse. Thèse de Doctorat 2003, Institut National Polytechnique de Toulouse, UMRCNRS N° 5828.
- [4] C. C. Chan and K. T. Chau: "An Overview of power Electronics in Electric Vehicles", IEEE Trans. On Industrial Electronics, Vol, 44, No 1, February 1997, pp.3-13.
- [5] C. PERTUZA: "Contribution à la définition de moteurs à aimants permanents pour un véhicule électrique routier". Thèse de docteur de l'Institut National Polytechnique de Toulouse, Février 1996.
- [6] S. TOUNSI, R. NEJI, F. SELLAMI: "Contribution à la conception d'un actionneur à aimants permanents pour véhicules électriques en vue d'optimiser l'autonomie". Revue Internationale de Génie Electrique, Volume 9/6-2006, pp. 693-718. Edition Lavoisier.
- [7] S. Tounsi : "Modélisation et Optimisation de la Motorisation et de l'Autonomie d'un Véhicule Electrique".Thèse de docteur de l'Ecole National d'Ingénieur de Sfax Tunisie, February 2006.
- [8] Sid Ali. RANDI: Conception systématique de chaînes de traction synchrones pour véhicule électrique à large gamme de vitesse. Thèse de Doctorat 2003, Institut National Polytechnique de Toulouse, UMRCNRS N° 5828.
- [9] S. TOUNSI, R. NEJI and F. SELLAMI : Electric vehicle control maximizing the autonomy: 3rd International Conference on Systems, Signal & Devices (SSD'05), SSD-PES 102, 21-24 March 2005, Sousse, Tunisia.